International Journal of Earth Sciences (2024) 113:319–333
https://doi.org/10.1007/s00531-023-02373-8

ORIGINAL PAPER

# In situ white mica Rb/Sr geochronology of the Leszczyniec metaigneous complex, West Sudetes: evidence of upper plate deformation at the onset of Variscan collision

Maria Młynarska[1] · Christopher J. Barnes[2] · Thomas Zack[3,5] · Jarosław Majka[1,4] · Stanisław Mazur[2]

Received: 4 April 2023 / Accepted: 27 November 2023 / Published online: 10 January 2024


## Abstract

The Karkonosze-Izera Massif in the West Sudetes preserves evidence of subduction of the Saxothuringian Ocean beneath the Teplá-Barrandian Domain. Within the massif, the Leszczyniec metaigneous complex (LMC) is identified as the upper allochthon. It exhibits a unique structural history in comparison to the underlying allochthons, suggesting that the LMC records a distinctive tectonic history. To investigate the timing of this history, two orthogneisses were studied from a single outcrop of the LMC for in situ white mica Rb/Sr geochronology. The outcrop bears a southeast-dipping foliation (S1) and a north/northeast plunging stretching lineation (L1), defined by white mica and quartz. Quartz recrystallization textures, white mica chemistry (celadonite content of 0.23–0.47), preservation of igneous plagioclase phenocrysts, and the metamorphic mineral assemblage, all indicate maximum epidote–amphibolite facies conditions. Single-spot Rb/Sr dates were calculated from white mica using initial $^{87}Sr/^{86}Sr$ values obtained by titanite and epidote. Results are similar for both rocks, providing weighted averages of 352.4 ± 4.1 Ma (MSWD: 0.6; n: 24) and 349.3 ± 2.5 Ma (MSWD: 0.4; n: 31). The rocks are interpreted to have the same structural and metamorphic history; thus, a pooled weighted average of 350.1 ± 5.3 Ma (2σ) is reported as the timing of white mica (re)crystallization during S1 and L1 development in epidote–amphibolite facies conditions. This event is bracketed by the timing of blueschist-facies metamorphism for the subjacent middle (c. 364 Ma) and lower (c. 345–341 Ma) allochthons, associated with an east/southeast-plunging L1. Considering the different structural and metamorphic histories of the LMC compared to the subjacent allochthons, it is likely that the complex was extracted from the Teplá-Barrandian upper plate due to subduction erosion prior to collective exhumation and stacking of the Karkonosze-Izera Massif.

**Keywords** Variscan orogeny · Karkonosze-Izera Massif · Leszczyniec metaigneous complex · In situ white mica Rb/Sr geochronology

## Introduction

The Leszczyniec metaigneous complex (LMC) occupies a small but important metamorphic terrane within the Karkonosze-Izera Massif of the West Sudetes at the northern margin of the Bohemian Massif (Fig. 1; Mazur and Aleksandrowski 2001). It represents the upper allochthon of a sequence of metamorphic units collectively referred to as the Karkonosze-Izera Massif (Mazur 1995; Žáčková et al. 2010; Jeřábek et al. 2016). Thrusting of these units occurred during the

✉ Christopher J. Barnes
cjbarnes063@gmail.com

Maria Młynarska
mkmlynarska@gmail.com

Thomas Zack
thomas.zack@gu.se

Jarosław Majka
jaroslaw.majka@geo.uu.se

Stanisław Mazur
ndmazur@cyf-kr.edu.pl

[1] Faculty of Geology, Geophysics and Environmental Protection, AGH University of Kraków, Kraków, Poland

[2] Institute of Geological Sciences, Polish Academy of Sciences, Kraków, Poland

[3] Department of Earth Sciences, University of Gothenburg, Göteborg, Sweden

[4] Department of Earth Sciences, Uppsala University, Uppsala, Sweden

[5] Department of Earth Sciences, University of Adelaide, Adelaide, Australia

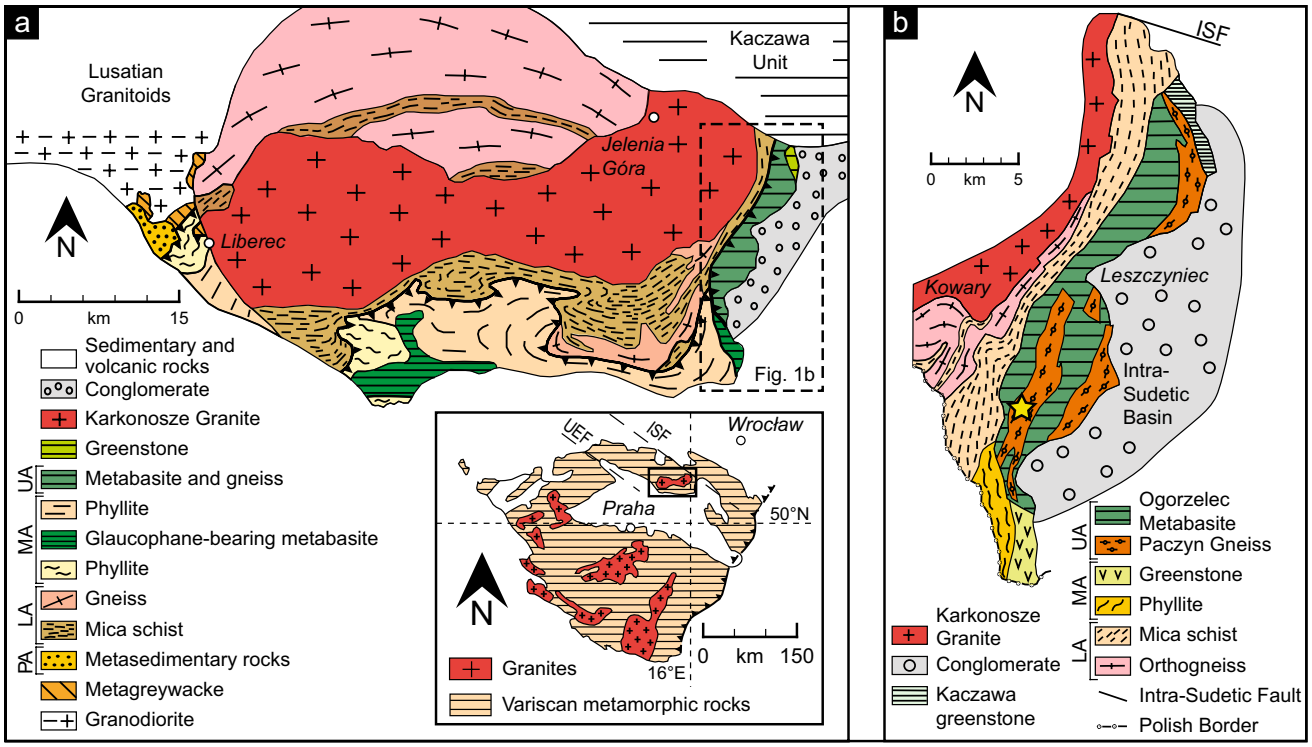


**Fig. 1** a Geological map of the Karkonosze-Izera Massif in the West Sudetes (modified after Mazur and Aleksandrowski 2001; Majka et al. 2016), presenting the extents of the parautochthon (PA), lower allochthon (LA), middle allochthon (MA), and upper allochthon (UA) surrounding the Karkonosze Granite. The upper allochthon is defined by the Leszczyniec metaigneous complex. The location of the Karkonosze-Izera Massif within the Bohemian Massif is presented in the inset map relative to Praha (Czechia) and Wrocław (Poland). **b** Geological map of the Leszczyniec metaigneous complex and surrounding rock units. The location of the Leszczyniec metaigneous complex within the Karkonosze-Izera Massif is indicated by the dashed black box in map a. The yellow star indicates the approximate location of the studied outcrop

Variscan orogeny, representing closure of the Saxothuringian Ocean leading to collision between the Saxothuringian and Teplá-Barrandian domains. The LMC bears a unique tectonic history as it preserves a structural fabric, related to epidote–amphibolite facies metamorphism, that is distinct from the underlying blueschist-facies allochthons of the Karkonosze-Izera Massif (Mazur and Kryza 1996; Mazur and Aleksandrowski 2001). However, the timing of the structural and metamorphic history of the complex has not been established. This information is critical for understanding the closure of the Saxothuringian Ocean and subsequent accretion of the Variscan belt of Central Europe.

The structural fabric of the LMC is defined by white mica-bearing orthogneisses and has been interpreted to have formed in epidote–amphibolite facies conditions (Kryza and Mazur 1995). This history warrants the application of white mica Rb/Sr geochronology as the closure temperature of this system (≥ 600 °C; Glodny et al. 1998) is above the inferred peak temperature conditions of the complex, allowing for the timing of white mica (re)crystallization associated with the structural fabric development to be resolved. White mica Rb/Sr geochronology is increasingly being conducted in situ with the use of laser ablation inductively coupled mass spectrometry, using two mass spectrometers separated by a gas reaction cell (hereafter referred to as LA-ICP-MS/MS). This apparatus is advantageous to resolve isobaric interferences of parent-daughter isotopes of beta-decay systems (Zack and Hogmalm 2016; Hogmalm et al. 2017). Using in situ laser ablation also allows for calculation of single-spot dates using an initial $^{87}Sr/^{86}Sr$ value derived from concomitant Ca-bearing phases (Rösel and Zack 2022). Therefore, in situ white mica Rb/Sr geochronology is applied to two orthogneisses of the LMC to resolve the timing of its tectonic history in the context of the collective Karkonosze-Izera Massif allochthons. Due to the novelty of the technique, the two investigated orthogneisses were obtained from the same outcrop to test the reproducibility of calculating single-spot white mica Rb/Sr dates for two different rocks that experienced the same structural and metamorphic history.

## Geological background

The Karkonosze-Izera Massif is exposed in the West Sudetes, located in the northern part of the Bohemian Massif (Fig. 1a; Franke et al. 1993; Narębski 1994; Franke and Żelaźniewicz 2000). The massif comprises several thrust sheets representing a subduction-accretion complex that records subduction of the Saxothuringian Ocean leading to collision between the Saxothuringian and Teplá-Barrandian domains during the Variscan Orogeny (Mazur and Aleksandrowski 2001; Konopásek et al. 2019). The terranes from bottom to top are defined as: (1) parautochthon; (2) lower allochthon; (3) middle allochthon; and (4) upper allochthon (Mazur and Kryza 1996; Mazur and Aleksandrowski 2001; Žáčková et al. 2010; Jeřábek et al. 2016). The upper allochthon is also referred to as the LMC (Fig. 1b; Kryza and Mazur 1995). The collective terranes were intruded by the Karkonosze Granite in late Carboniferous time (Machowiak and Armstrong 2007; Žák et al. 2013; Kryza et al. 2014).

The parautochthon constitutes (meta)granitoid rocks with late Cambrian/Early Ordovician protolith ages (Kröner et al. 2001; Zieger et al. 2018), as well as sedimentary rocks of the Ještěd unit (Chaloupský 1989; Chlupáč 1993; Kachlík and Kozdrój 2001). The lower and middle allochthons both comprise various metasedimentary rocks and orthogneiss (the latter only in the lower allochthon), which are interpreted to represent the proximal and distal portions of the former Saxothuringian passive margin, respectively (Winchester et al. 2003; Oberc-Dziedzic et al. 2010), with relics of the Saxothuringian oceanic crust (Patočka and Pin 2005). Rocks in both allochthons were metamorphosed in blueschist-facies conditions (Smulikowski 1995; Žáčková et al. 2010; Faryad and Kachlík 2013; Majka et al. 2016; Jeřábek et al. 2016). The conditions of metamorphism are generally similar, the lower allochthon subjected to $\geq$ 1.8–1.9 GPa and 460–520 °C (Žáčková et al. 2010), and several rocks of the middle allochthon altogether recording 1.2–2.0 GPa and 400–540 °C (Faryad and Kachlík 2013; Majka et al. 2016; Jeřábek et al. 2016). However, the timing of the metamorphic events is different. Metamorphism of the lower allochthon was originally dated by monazite (Th-) U–Pb to 330 ± 10 Ma and 328 ± 6 Ma (Žáčková et al. 2010), but more recent garnet Lu–Hf and monazite U–Pb geochronology provided dates of 345 ± 1 Ma, 342 ± 7 Ma, and 341 ± 3 Ma, indicating an older metamorphic history (Konopásek et al. 2019). The middle allochthon was metamorphosed earlier, resolved by a garnet Lu–Hf date of 364 ± 1 Ma (Konopásek et al. 2019). However, Konopásek et al. (2019) also dated chloritoid-bearing phyllites of the middle allochthon providing monazite Concordia ages of 336.5 Ma. Previous $^{40}Ar/^{39}Ar$ geochronology of white mica, biotite, and hornblende have provided a range of dates for both allochthons. For the lower allochthon, dates are dispersed from 340 ± 6 Ma to 323 ± 6 Ma (Marheine et al. 2002). For the middle allochthon, dates range from 364 ± 2 Ma to 313 ± 3 Ma (Malusky and Patočka 1997; Marheine et al. 2002). For both allochthons, these dates were interpreted to reflect blueschist-facies metamorphism, subsequent exhumation and retrogression, and final tectonic activity related to emplacement of the Karkonosze Granite. Structural fabrics associated with high-pressure metamorphism and subsequent retrogression during exhumation were detailed by Mazur and Kryza (1996), Mazur and Aleksandrowski (2001) and Jeřábek et al. (2016). The foliations of the lower and middle allochthons in the eastern part of the Karkonosze-Izera Massif are typically observed to be moderately to steeply dipping towards the east to southeast and, locally, to northwest on the overturned limbs of folds. High-pressure metamorphism is associated with a southeast-plunging lineation (L1) with top-to-northwest sense of shear. The lineation associated with exhumation of the allochthons (L2) plunges towards the east/southeast with a top-to- east/southeast shear sense.

The upper allochthon of the Karkonosze-Izera Massif is represented by the LMC. The complex is composed of both mafic rocks and felsic to intermediate orthogneisses, also referred to as the Ogorzelec Metabasite and the Paczyn Gneiss, respectively (Kryza and Mazur 1995). Zircon U–Pb geochronology has resolved the metaigneous complex protolith rocks to late Cambrian in age (Oliver et al. 1993; Kozdrój et al. 2005). The conventional interpretations of the protolith rocks are that they represent a relic terrane of the Saxothuringian Ocean (Narębski et al. 1986; Szałamacha and Szałamacha 1991) or a former continental rift floored by oceanic crust (Kryza et al. 1995; Winchester et al. 1995). Quantitative pressure–temperature and geochronological studies of metamorphism and deformation are completely lacking for the LMC. However, detailed petrography of the rocks indicates that the highest grade of metamorphism was in the epidote–amphibolite facies (Kryza and Mazur 1995). Amphiboles within the intermediate orthogneisses show distinct zoning with actinolite cores surrounded by hornblende rims. Epidote and white mica compositions are also consistent with metamorphism in the epidote–amphibolite facies. The foliation of the LMC (S1) is related with epidote–amphibolite facies metamorphism and steeply dips towards the east, southeast and northwest (Fig. 2), similar the lower and middle allochthons (Mazur and Kryza 1996; Mazur and Aleksandrowski 2001). However, epidote–amphibolite facies metamorphism is associated with a distinct northeast or southwest plunging lineation (L1; Fig. 2) with a top-to-southwest (sinistral) sense of shear, contrasting the underlying units (Mazur 1995; Mazur and Aleksandrowski 2001). This lineation is defined in the felsic Paczyn Gneiss

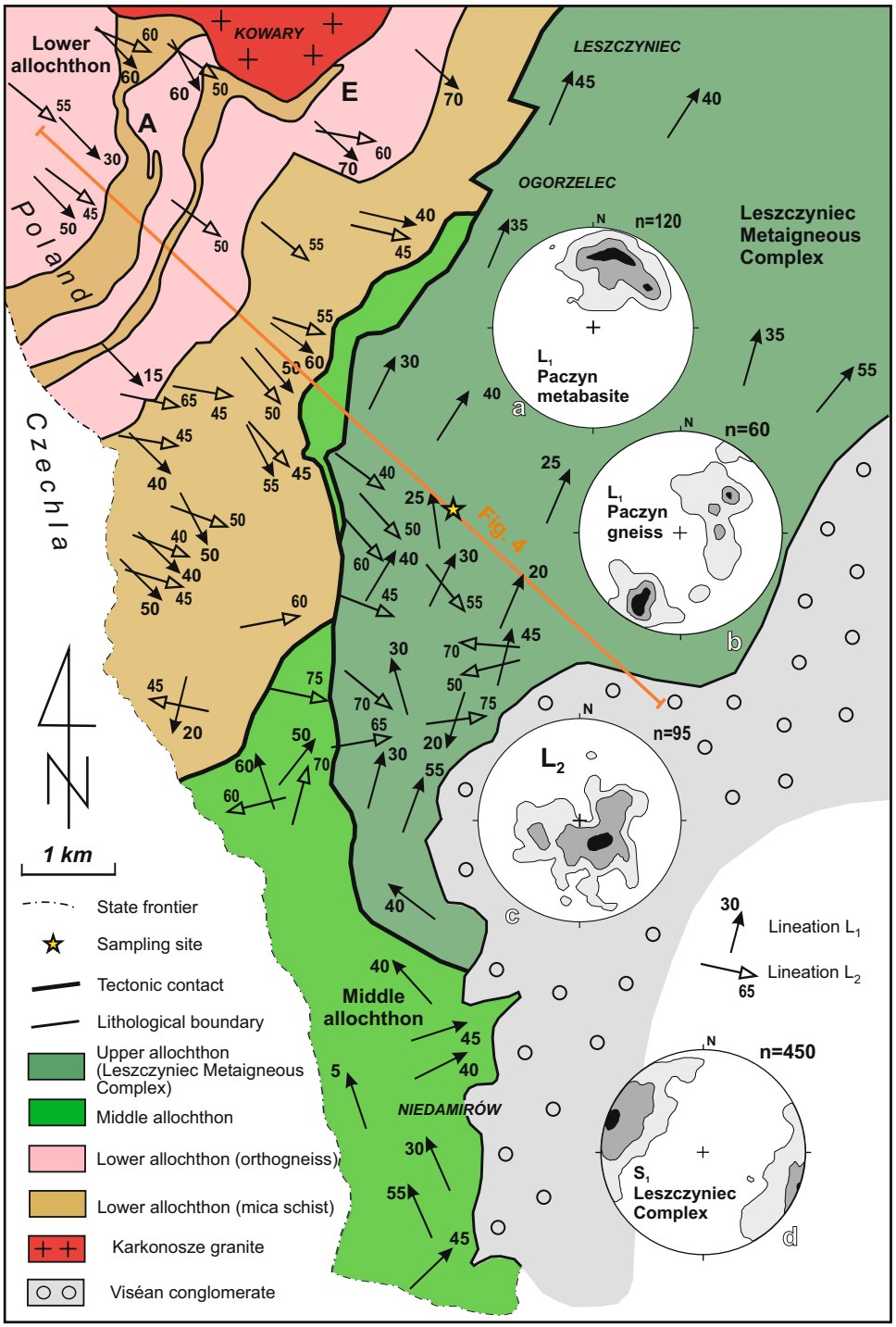


**Fig. 2** Tectonic map for the southern part of the Leszczyniec metaigneous complex and adjacent units based on the compilation of data from Mazur (1995) and recent observations. Stereoplots show: **a** Lineation L1 in the Leszczyniec metabasites; **b** Lineation L1 in the Paczyn orthogneisses; **c** Lineation L2 in both the metabasites and orthogneisses; **d** foliation S1 in both the metabasites and orthogneisses. Contour lines in the density plots are at 1, 4, 6% (plots **a** and **b**); 1, 3, 8% (plot **c**) and 1, 3, 6% (plot **d**)

by alignment of white mica and elongation of recrystallized quartz, including partially recrystallized quartz augens. Final exhumation of the LMC relates with an east/southeast-plunging lineation (L2) and top-to-east/southeast (dip-slip) shear sense, reflecting the subjacent allochthons (Mazur 1995; Mazur and Aleksandrowski 2001). In some locations, both lineations are superimposed on foliation S1 with L1 and L2 corresponding to a mineral stretching lineation and crenulation axis, respectively (Fig. 3a). In the intermediate variety of the orthogneisses, often anastomosing crenulations overlap the mineral lineation marked by the parallel arrangement of hornblende crystals (Fig. 3b). A nearly perpendicular orientation of L1 and L2 (Fig. 3) in the LMC is confirmed at a regional scale by cumulative stereoplots (Fig. 2). The latter also show a wider dispersion of L1 in the orthogneisses than in the mafic rocks. The contacts between the two are strongly sheared but

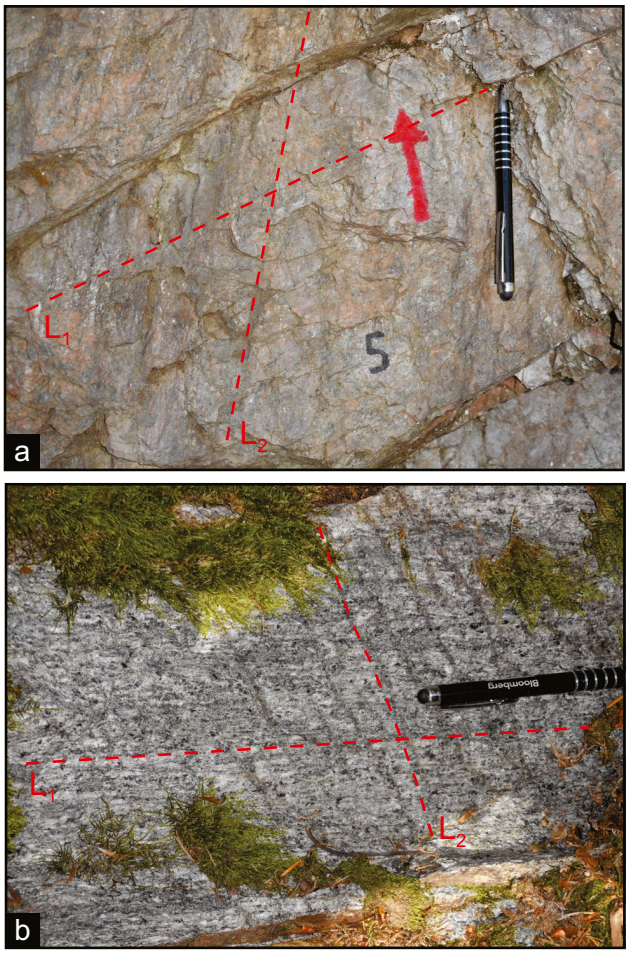


**Fig. 3** Field photos showing structural relationships in the southern part of the Leszczyniec metaigneous complex. **a** Lineations L1 and L2 superimposed on foliation S1, corresponding to a mineral stretching lineation and crenulation axes, respectively. Photograph taken at the sampled exposure of the felsic Paczyn orthogneiss (GPS coordinates: N50.738935; E15.870180). **b** Anastomosing crenulations L2 overlap mineral lineation L1 marked by the parallel arrangement of hornblende crystals. Intermediate Paczyn orthogneiss (N50.746448; E15.923601). The length of the pencil in both photos is 17 cm

sometimes preserve an intrusive character. Although lineation L2 in the LMC is mostly manifested as crenulations or mesoscopic folds in the adjacent quartz-muscovite schists of the lower allochthon it is associated with pronounced top-to-east/southeast (dip-slip) kinematic indicators.

## Methods

### Sampling and characterization

Two white mica-bearing felsic orthogneisses (samples LC22-05 and LC22-06) were obtained from an outcrop of the Paczyn Gneiss in the LMC (Figs. 1, 2). The position of the sampling site within the verticalized nappe stack is shown by the cross-section of Fig. 4. The structurally uppermost LMC is also located on the hanging wall of the ductile normal-displacement dip-slip shear zone localised within the quartz-muscovite schists of the lower allochthon (Fig. 4). The shear zone activity was associated with development of lineation L2. Different sections (approximately ten meters apart) of the felsic Paczyn Gneiss outcrop were sampled (Fig. 5). These rocks were chosen to resolve the timing of amphibolite facies metamorphism and directly compare the reproducibility of calculating in situ single-spot Rb/Sr dates using measured initial $^{87}Sr/^{86}Sr$. Standard 30 µm thin sections were cut from both rocks for transmitted light microscopy to characterize mineralogy and microstructures in the rocks. Thick sections (250 µm) were also cut from the same rock chips as the thin sections for purpose of in situ white mica Rb/Sr geochronology. The thick sections were imaged in back-scattered electron (BSE) images using a JEOL JXA8530F electron microprobe at Uppsala University (Uppsala, Sweden). Photomosaics of BSE images were obtained for areas of interest for geochronological analysis to show the associations between microstructures defined by white mica that mimicked those observed in thin section. After electron microprobe analysis, reflected light images were obtained for the areas of interest in the thick sections to use as navigational maps for programming in situ analyses.

### LA-ICP-MS/MS

In situ white mica Rb/Sr geochronology was conducted at the Microgeochemistry Laboratory at the Department of Earth Sciences, University of Gothenburg. An ESI 213NWR laser apparatus connected to an Agilent 8800 ICP-QQQ was used for ablation and measurement, following the methods and protocols developed by Zack and Hogmalm (2016), Hogmalm et al. (2017), and Rösel and Zack (2022). A laser spot with a diameter of 50 µm was used for ablation of white mica and 30 µm for ablation of titanite and epidote. The laser was pulsed with a frequency of 10 Hz and the fluence was 5.3 J/cm$^{-2}$. Helium was used as the carrier gas (750 ml/m) and was mixed with nitrogen (4 ml/m), then with argon (700–800 ml/m). The entire gas-sample mixture was directed through a glass cylinder (20 cm in length with 2 cm diameter) filled with 11 g of steel wool to remove larger particles and enhance signal stability (Hu et al. 2012). The mixture was introduced into a gas reaction cell with $N_2O$ for purpose of reacting with Sr isotopes derived from the ablated material (for details, see Hogmalm et al. 2017).

All analyses were conducted over a single analytical session. The primary reference material for geochronological analysis was MicaMg nanopellet powder and was also used along with both NIST610 and BCR-2G glasses as primary reference materials for major and trace elements. To monitor

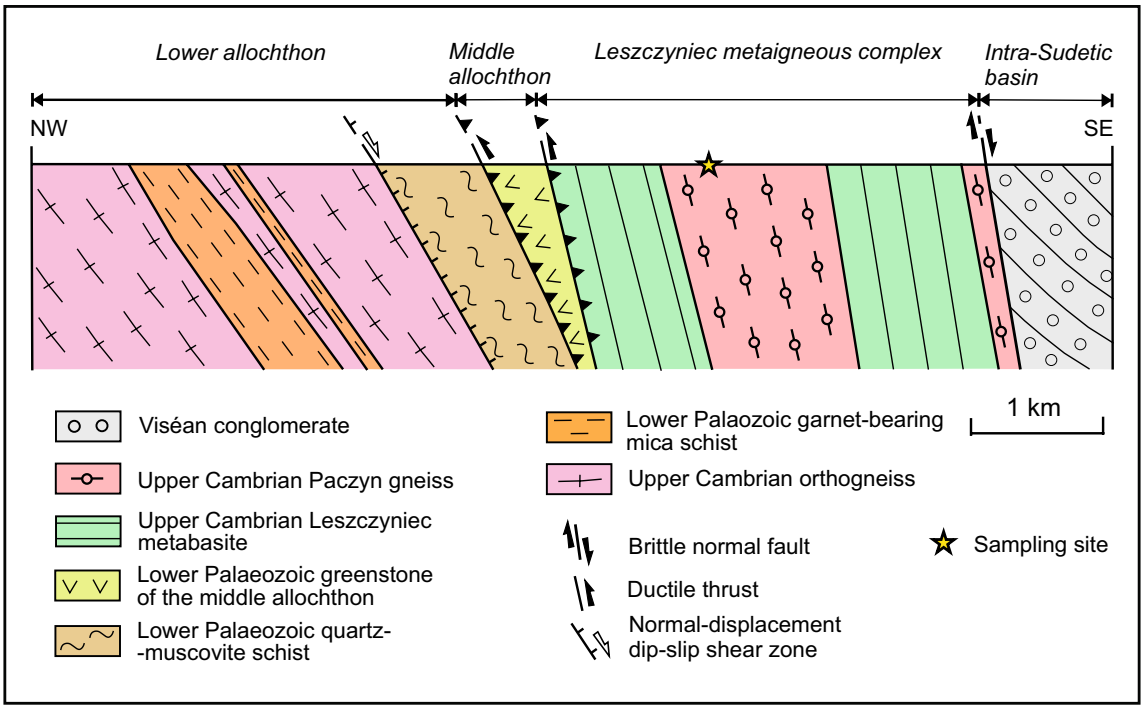


**Fig. 4** Cross-section through the southern part of the Leszczyniec metaigneous complex and adjacent units, showing the position of the sampling site within the structure of the upper, middle and lower allochthons of the Karkonosze-Izera Massif. See Fig. 2 for location

the stability of the measurements over the analytical session, secondary reference materials were routinely analysed, interspersed throughout cycles of 12 unknown measurements. The secondary reference materials were MicaFe nanopellet powder, Högsbo white mica, GA1550 biotite, biotite from the Wilsons Promontory Batholith, and La Posta biotite. The literature ages for the primary and secondary reference materials are reported in Table 1. More details for these reference materials can be found in Rösel and Zack (2022), and the protocol for measuring and recalculating $^{87}$Rb, $^{86}$Sr, and $^{87}$Sr are also detailed in the same publication. In addition, major and trace elements (Li, Na, Mg, Al, Si, P, K, Ca, Ti, V, Cr, Mn, Fe, Zn, Y, Zr, Nb, Cs, Ba, Ce, Tl) were gathered simultaneous to the Rb and Sr isotopes. The data reduction was performed using Iolite v. 3.71 (Paton et al. 2011) using an in-house built data reduction scheme and developed protocol for Rb/Sr geochronology (Rösel and Zack 2022). Each analysis of reference materials and unknowns were scrutinized using raw $^{85}$Rb/$^{86}$Sr, raw $^{85}$Rb/$^{87}$Sr, and raw $^{87}$Sr/$^{86}$Sr, along with element counts. Specifically, analyses with > 10,000 CPS of Ca were discarded due to potential contamination of apatite, titanite, or epidote. Integrations were defined according to these ratios and element counts to remove any irregular signal. Entire analyses were discarded if they were overall poor (less than ~ 12 s of useable signal). Single-spot dates were calculated from the accepted unknown analyses using initial $^{87}$Sr/$^{86}$Sr ratios obtained from titanite and epidote in the unknown samples. The chemistry of the single-spots was computed from the same integrations using an in-house built Excel spreadsheet that recalculates major and trace element concentrations (µg/g) using the results of the primary reference materials. Further processing of the reduced data was conducted with IsoplotR online (Vermeesch 2018).

## Results

### Rock descriptions

The outcrop of the orthogneisses is well-foliated (018/71 SE) and bears a stretching lineation (03-017) defined by quartz and white mica. A crenulation (axis of 68-121) is also observed on the foliation plane, oblique to the stretching lineation. The two rocks show no obvious lithological differences at the outcrop. Thin sections obtained from both rocks demonstrate that they are predominantly composed of quartz and plagioclase with white mica, epidote, titanite, apatite, rutile, chlorite, zircon, and hematite (Fig. 5). Matrix quartz is pervasively recrystallized (typically 50–500 µm in length), often showing shape preferred orientations defining the rock foliations. Large, partially recrystallized quartz augens (up to 5 mm in length) also remain within the recrystallized quartz-dominated matrix. Plagioclase is found as large (up

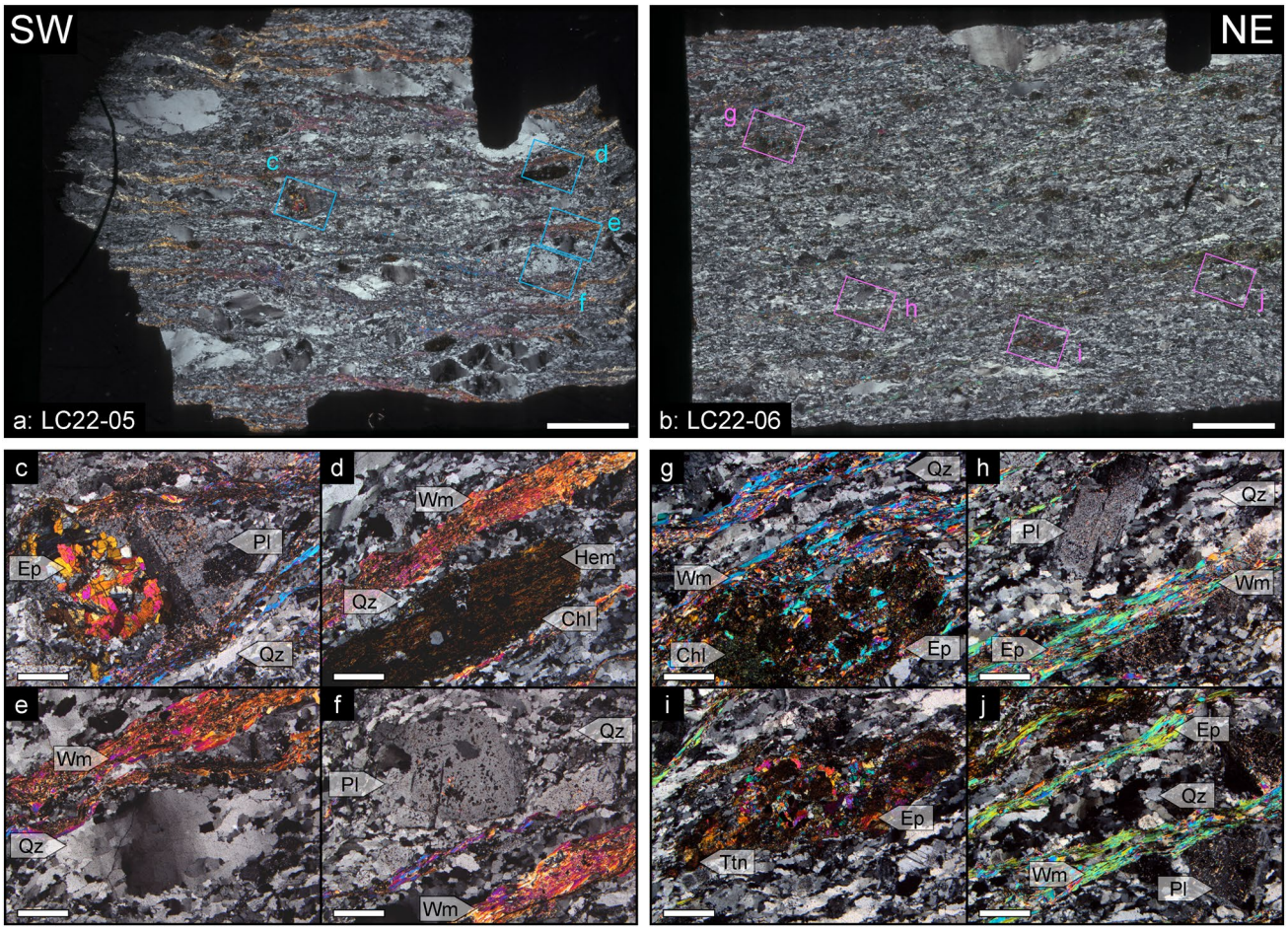


**Fig. 5** **a**, **b** Transmitted light and **c**–**j** cross-polarized light microphotographs of the studied orthogneiss samples. Thin sections were cut perpendicular to S1 and parallel to L1. All scale bars in a and b are 5 mm, and in **c**–**j** are 500 µm. **a** and **b**: Thin section scan images of LC22-05 (left) and LC22-06 (right). The microphotographs presented below the images are located by the blue boxes. The orientations of the microphotographs were rotated with respect to the scan images to better illustrate the mineral assemblages and textures. **c** Coarse-grained lens of epidote and plagioclase enveloped by bands of white mica, fine-grained epidote, and recrystallized quartz. The coarse epidote is highlighted in Fig. 6a. **d** White mica/epidote bands and recrystallized quartz surrounding an ovoid mass of quartz, plagioclase, chlorite, and iron oxide. **e** Coarse-grained recrystallized quartz augen enveloped by fine-grained recrystallized quartz and white mica/epidote bands. **f** Tabular plagioclase grains with fine-grained recrystallized quartz and white mica/epidote bands. **g** Agglomerate of chlorite, epidote, white mica, apatite, and iron oxide within the matrix of fine-grain recrystallized quartz and white mica/epidote bands. The mineral agglomerate is highlighted in Fig. 6b. **h** Tabular plagioclase grain surrounded by fine-grain recrystallized quartz and white mica/epidote bands. **i** Agglomerate of titanite, epidote, chlorite, apatite, and white mica within the fine-grain recrystallized quartz matrix. The mineral agglomerate is highlighted in Fig. 6c. **j** Tabular plagioclase enveloped by fine-grain recrystallized quartz and white mica/epidote bands

to 1.2 mm in diameter), tabular grains that are sometimes twinned and lack evidence of significant recrystallization. The plagioclase grains are partially replaced by white mica and epidote. Although both rocks portray similar quartz and plagioclase characteristics, LC22-05 is overall coarser and augens are more common compared to LC22-06. White mica are often found as small grains (typically < 250 µm in length) along continuous bands (up to 600 µm thick) defining the rock foliation. Both rocks have a similar modal abundance of white mica, but LC22-05 generally has finer grains but thicker bands compared to LC22-06, which shows slightly more isolated but coarser grains. An abundance of epidote (typically 20–150 µm in diameter) is also found within the bands of white mica in both rocks. The bands anastomose around the quartz augens, plagioclase, as well as mineral agglomerates (up to 3 mm long) of chlorite, epidote, rutile, titanite, apatite, zircon, and hematite (Figs. 5, 6b). Chlorite is only found in the agglomerates and not observed to replace white mica.

## White mica chemistry and Rb/Sr geochronology

Single-spot dates were calculated from the secondary reference materials using reported initial $^{87}Sr/^{86}Sr$ values (see

**Table 1** Comparison of measured versus literature values for reference materials

| | MicaMg | MicaFe | Högsbo | GA1550 | Wilsons Promontory | La Posta |
|---|---|---|---|---|---|---|
| Material | Nanopellet powder | Nanopellet powder | Muscovite | Biotite | Biotite | Biotite |
| Measured ages | 519.0 ± 1.7 Ma (MSWD: 1.7, n: 21) | 293.1 ± 0.9 Ma (MSWD: 0.8, n: 10) | 1038.2 ± 4.3 Ma (MSWD: 3.8, n: 9) | 100.6 ± 2.8 Ma (MSWD: 1.0, n: 9) | 382.2 ± 6.8 Ma (MSWD: 19, n: 8) | 85.2 ± 1.7 Ma (MSWD: 1.2, n: 7) |
| Literature ages | 519.4 ± 6.5 Ma (*Compiled ages*)[a]<br>519.7 ± 1.3 Ma (*Nanopellet powder Rb/Sr*)[b] | 299 ± 4 Ma (*Biotite $^{40}Ar/^{39}Ar$*)[c]<br>305.4 ± 2.0 Ma (*Nanopellet powder Rb/Sr*)[b]<br>307.6 ± 0.4 Ma (*Muscovite $^{40}Ar/^{39}Ar$*)[d] | 1023.8 ± 4 Ma (*Muscovite Rb/Sr*)[b]<br>1029 ± 1.7 Ma (*Columbite Pb/Pb*)[e]<br>1037 ± 11 Ma (*Muscovite nanopowder Rb/Sr*)[a] | 99.1 ± 0.1 Ma (*Zircon U–Pb*)[f]<br>99.2 ± 0.1 Ma (*Biotite $^{40}Ar/^{39}Ar$*)[g]<br>99.8 ± 1.9 Ma (*Biotite Rb/Sr*)[b]<br>100.3 ± 1.9 Ma (*Biotite Rb/Sr*)[h]<br>100.4 ± 0.7 Ma (*Biotite Rb/Sr*)[i] | 397.2 ± 2.7 Ma (*Zircon U–Pb*)[j] | 89.2 ± 1.0 Ma (Biotite Rb/Sr)[b]<br>91.6 ± 1.2 Ma (*Compiled age*)[k] |

[a]Hogmalm et al. (2017)
[b]Rösel and Zack (2022)
[c]Redaa et al. (2022)
[d]Grove and Harrison (1996)
[e]Romer and Smeds (1994)
[f]Schoene et al. (2006)
[g]Phillips et al. (2017)
[h]Li et al. (2008)
[i]Williams et al. (1982)
[j]Clemens et al. (2023)
[k]Zack and Hogmalm (2016)

Rösel and Zack 2022; Table S1). The initial $^{87}Sr/^{86}Sr$ value for Wilsons Promontory was taken as 0.7088 from Waight et al. (2000). The results are: MicaFe nanopellet powder (293.1 ± 0.9 Ma, MSWD: 0.8, n: 10), Högsbo white mica (1038.2 ± 4.3 Ma, MSWD: 3.8, n: 9), GA1550 biotite (100.6 ± 2.8 Ma, MSWD: 1.0, n: 9), Wilsons Promontory biotite (382.2 ± 6.8, MSWD: 19, n: 8), and La Posta biotite (85.1 ± 1.7 Ma, MSWD: 1.2, n: 7). The weighted averages are either equivalent to the literature ages or slightly younger (Table 1).

Thirty-nine in situ laser ablation analyses were conducted for orthogneiss LC22-05, and forty-one for orthogneiss LC22-06 on foliation-defining white mica (Table S1). Based on criteria outlined in the methodology, twenty-four out of thirty-nine analyses were accepted for LC22-05, and thirty-one out of forty-one were kept for LC22-06. Chemistry of the white mica in both orthogneisses was recalculated to white mica endmembers (Fig. 7, Table S1; Coggon and Holland 2002). The white mica chemistry for LC22-05 ranges from $X_{Ms}$: 0.42–0.60 (avg. 0.55) and $X_{Cel}$: 0.23–0.43 (avg. 0.29). White mica in LC22-06 show overlapping composition and range with $X_{Ms}$: 0.40–0.55 (avg. 0.51) and $X_{Cel}$: 0.31–0.47 (avg. 0.36). Although the overall chemistry overlaps, the majority of single-spot compositions are distinct between the two rocks, with mica from LC22-05 being more enriched and more depleted in $X_{Ms}$ and $X_{Cel}$, respectively, compared to LC22-06 (Fig. 7).

Single-spot Rb/Sr dates were calculated from the results of the same analyses (Fig. 8). No correlations between major or trace element chemistry and Rb/Sr dates are observed for either orthogneiss. To calculate single-spot dates, the initial $^{87}Sr/^{86}Sr$ values were obtained from titanite and epidote within the orthogneisses (Fig. 6; Table S2). For LC22-05, five analyses of titanite and five of epidote provided an initial $^{87}Sr/^{86}Sr$ weighted average of 0.7034 ± 0.0028 (Fig. 6e). No differences are observed between the ratios yielded by either mineral. The resulting single-spot dates range from 339 ± 20 to 368 ± 31 Ma (2σ) and define a weighted average of 352.4 ± 4.1 Ma (MSWD: 0.6; Fig. 8c). For LC22-06, eleven analyses of titanite yielded a weighted average initial $^{87}Sr/^{86}Sr$ of 0.7083 ± 0.0037 (Fig. 6f). The resulting single-spot dates range from 342 ± 15 Ma to 362 ± 14 Ma (2σ)

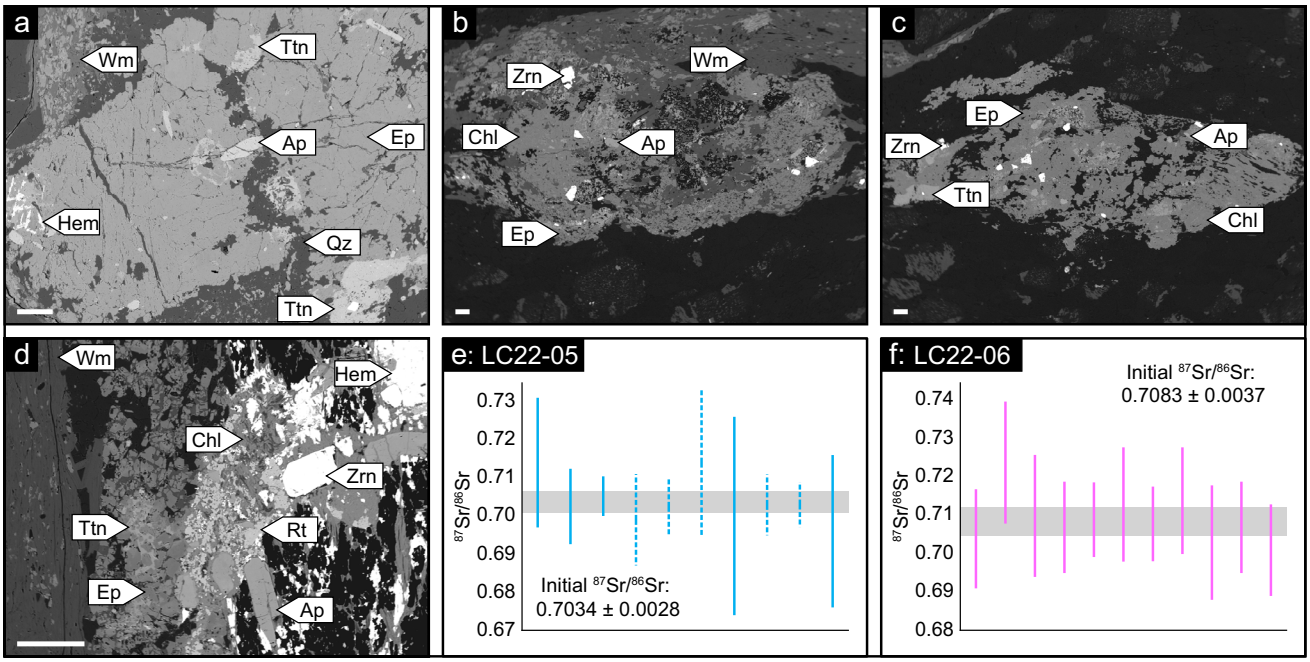


**Fig. 6** Back-scattered electron images highlighting mineral textures of mineral agglomerates in the orthogneisses (**a**–**d**) and initial $^{87}Sr/^{86}Sr$ values (**e**, **f**) obtained from Ca-bearing phases in the agglomerates. All scale bars in the back-scattered electron images are 100 µm. **a** Coarse epidote associated with apatite, titanite, and hematite. The titanite in the lower right surrounds a zircon grain. Fine epidote is present in the top left in a white mica band. Enlargement of Fig. 5c. **b** Mass of chlorite, epidote, and white mica with apatite and zircon flanked by a white mica/epidote band. Enlargement of Fig. 5g. The black areas within the agglomerate are empty spaces. **c** Epidote and chlorite containing apatite, zircon, and titanite. The highlighted titanite grain is enveloping a zircon grain. Enlargement of Fig. 5i. **d** Agglomerate of chlorite, epidote, rutile, and hematite with individual grains of apatite and zircon flanked by a white mica/epidote band. Titanite is present surrounding epidote. The black areas within the agglomerate are empty spaces. **e** and **f** Initial $^{87}Sr/^{86}Sr$ results from single-spot laser ablation of titanite (solid lines) and epidote (dashed lines) from orthogneisses LC22-05 and LC22-06. The individual bars represent the $^{87}Sr/^{86}Sr \pm 2\sigma$ uncertainty derived from a single laser ablation. The horizontal grey bar represents the average initial $^{87}Sr/^{86}Sr$, which is written for each graph

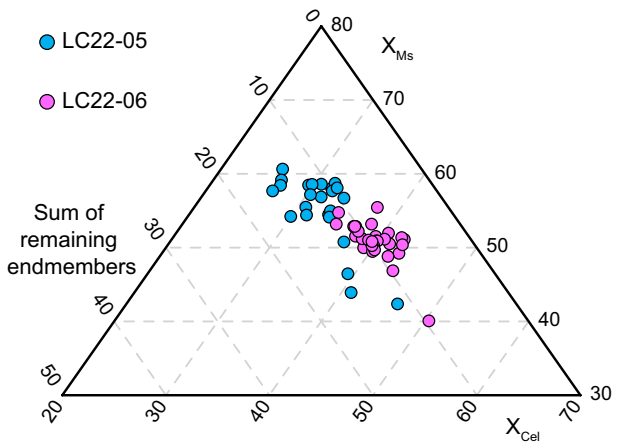


**Fig. 7** Ternary plot showing the single-spot chemical compositions of white mica provided by the in situ Rb/Sr geochronological analysis for the studied orthogneisses. The white mica chemistry was recalculated according to Coggon and Holland (2002). The upper vertex represents the muscovite endmember ($X_{Ms}$), the right vertex indicates the celadonite endmember ($X_{Cel}$), and the left vertex denotes the sum of remaining endmembers (Ti-phengite, $X_{Ti}$; paragonite, $X_{Pa}$, pyrophyllite, $X_{Py}$; margarite, $X_{Ma}$; and phlogopite, $X_{Phl}$)

and yield a weighted average of 349.3 ± 2.5 Ma (MSWD: 0.4; Fig. 8d). A pooled weighted average from both orthogneisses is 350.1 ± 5.3 Ma. The uncertainty is reported as 1.5% (2σ) of the pooled average, according to the minimum precision of the employed protocol as outlined in Rösel and Zack (2022). For comparison, ages were also calculated using the conventional Nicolaysen isochron approach for the two orthogneisses without initial $^{87}Sr/^{86}Sr$ values (Fig. 8e). For LC22-05, the date was calculated to 354.1 ± 18.3 Ma (MSWD: 0.3). For LC22-06, the result is 350.4 ± 20.2 Ma (MSWD: 0.1).

## Discussion

The southeast-dipping foliation (S1) of the studied outcrop bears a north/northeast plunging stretching lineation (L1) and southeast-plunging crenulation cleavage axis (L2). Elongation of quartz and white mica define the ductile S1 and L1 structural fabric of the orthogneisses. Previous studies of the LMC concluded these structures were related to

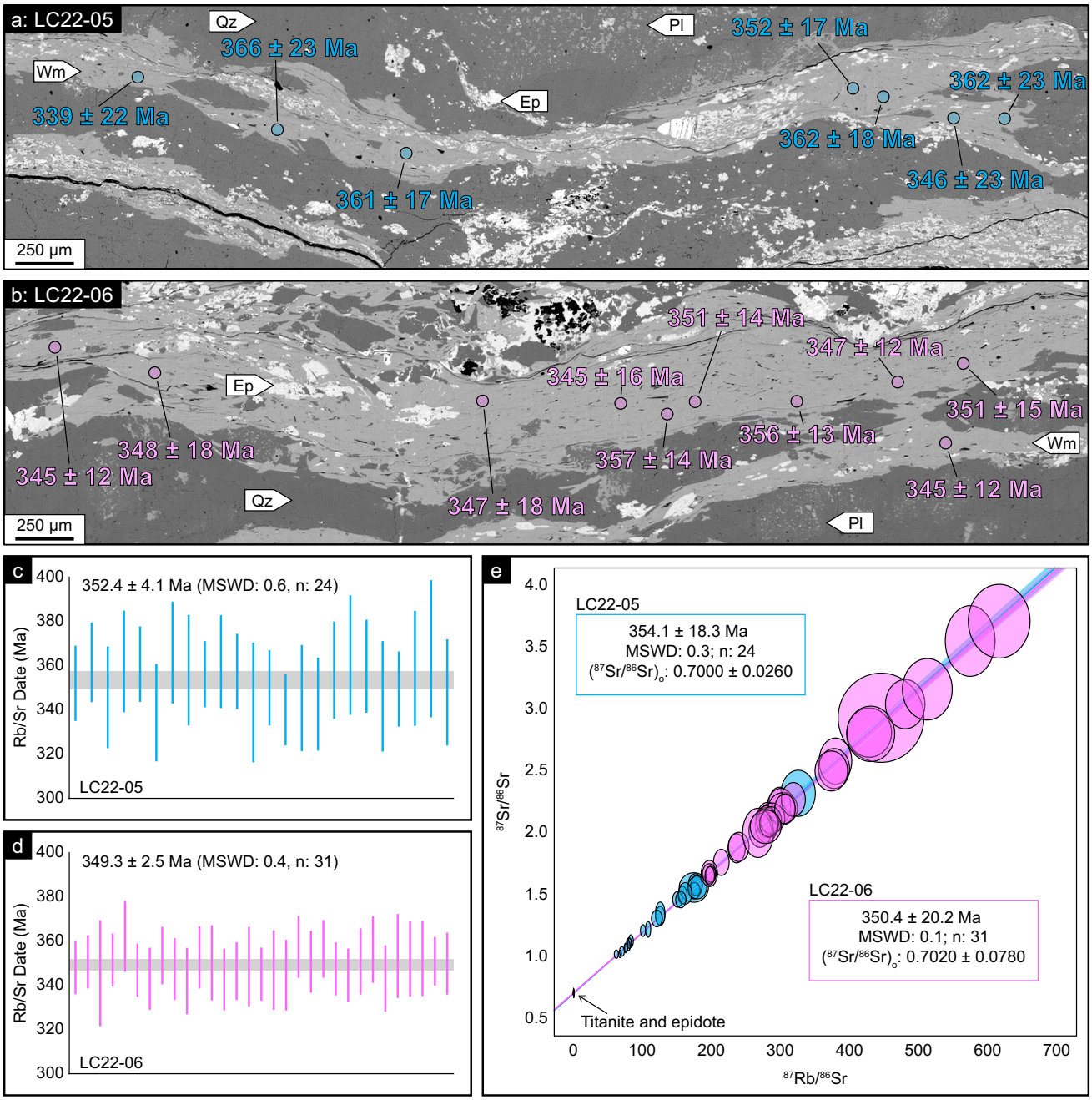


**Fig. 8** Presentation of the single-spot white mica Rb/Sr dates for the studied orthogneisses. **a** and **b** Back-scattered electron photomosaics of a white mica/epidote band in orthogneiss samples LC22-05 and LC22-06 showing in situ laser ablation locations and the resulting dates. **c** and **d** Single-spot Rb/Sr dates ± 2σ uncertainty for samples LC22-05 and LC22-06, represented by vertical bars. The Rb/Sr dates were calculated using the average initial $^{87}Sr/^{86}Sr$ values for each respective rock. The horizontal grey bars represent the average dates, which are provided at the top of each graph. The pooled weighted average is produced from the results of both orthogneisses and is presented as the age of epidote–amphibolite facies metamorphism. **e** Rb/Sr isochron plots showing the results of the two studied orthogneisses. The isochron dates were calculated for each orthogneiss individually and without initial $^{87}Sr/^{86}Sr$ values

epidote–amphibolite faces metamorphism (Kryza and Mazur 1995; Mazur and Aleksandrowski 2001), which are supported by several observations of the studied orthogneisses. Recrystallization textures of the matrix and augen quartz resemble subgrain rotation with possible bulging grain dynamic recrystallization. Although dependant on strain rates, these recrystallization mechanisms are typical of deformation in low to moderate temperatures (Fig. 5; Stipp et al. 2002). The tabular forms of plagioclase reflect primary igneous textures that were not recrystallized, indicating that

temperature conditions were likely ≤ 500 °C (Rosenberg and Stünitz 2003). White mica has a significant celadonite content that is usual for (re)crystallization in medium pressure conditions (Fig. 7; Massonne and Schreyer 1987). Lastly, the mineral agglomerates also appear to be pseudomorphs after igneous phenocrysts with significant Ca, Mg, and Fe content, and contain an abundance of epidote, which is also widespread throughout the white mica bands (Figs. 5, 6, 8). The white mica does not show replacement by chlorite (Fig. 6), indicating that the presence of chlorite along with epidote and titanite in the agglomerates is a function of the pseudomorph precursor compositional heterogeneities, as opposed to later-stage greenschist facies retrogression. Therefore, the formation of S1 and L1, defined by quartz and white mica is interpreted to have occurred in epidote–amphibolite facies conditions.

Different initial $^{87}Sr/^{86}Sr$ values were obtained from the two orthogneisses (Fig. 6). These differences are reflected in the variability of grain size (i.e., quartz augens, plagioclase phenocrysts, white mica) and white mica chemistry, demonstrating rheological and chemical differences between the two rocks (Figs. 5, 7). However, the titanite and epidote that provided the initial $^{87}Sr/^{86}Sr$ values are both interpreted to be concomitant with (re)crystallization of white mica defining S1 and L1. The weighted averages of single-spot dates for each rock are equivalent within 2σ uncertainty (352.4 ± 4.1 Ma and 349.3 ± 2.5 Ma; Fig. 8), which altogether indicates that white mica Rb/Sr records the same event in both rocks, regardless of the minor rheological or chemical differences. The weighted average values are comparable to both isochron dates calculated with initial $^{87}Sr/^{86}Sr$ values for the respective samples, however, the single-spot approach provides superior precision compared to the isochron (Fig. 8). The similarities demonstrate the reproducibility and reliability for calculating single-spot dates using initial $^{87}Sr/^{86}Sr$ from Ca-bearing phases concomitant with white mica (Rösel and Zack 2022). As the two rocks are interpreted to record the same event, a pooled weighted average of 350.1 ± 5.3 Ma is interpreted as the timing of white mica (re)crystallization associated with S1 and L1 development during epidote–amphibolite facies metamorphism.

The S1 and corresponding southeast-plunging L1 of the middle and lower allochthons, subjacent to the LMC (Fig. 1), were both metamorphosed in blueschist-facies conditions. The middle allochthon rocks were metamorphosed at 1.2–1.5 GPa and 480–520 °C (Majka et al. 2016) at c. 364 Ma (Konopásek et al. 2019), whereas lower allochthon metamorphism of ≥ 1.8–1.9 GPa and 460–520 °C occurred at c. 345–336.5 Ma (Malusky and Patočka 1997; Marheine et al. 2002; Žáčková et al. 2010; Faryad and Kachlík 2013; Jeřábek et al. 2016; Konopásek et al. 2019). Winchester et al. (2003) interpreted the middle and lower allochthon rocks as relics of the distal and proximal Saxothuringian passive margin, respectively. On the other hand, Patočka and Pin (2005) postulated an oceanic affinity for the blueschist-facies metabasites of the middle allochthon. Provided the margin geometry, along with timing and conditions of metamorphism, a sequence of events can be deduced (see tectonic model of Konopásek et al. 2019). The metabasites of the middle allochthon would have subducted first and reached blueschist conditions at c. 364 Ma. They would have been trailed by the remaining middle and lower allochthon rocks, attaining blueschist-facies metamorphism at c. 345–336.5 Ma. These two allochthons were exhumed together (Malusky and Patočka 1997; Mazur and Aleksandrowski 2001; Marheine et al. 2002; Žáčková et al. 2010; Konopásek et al. 2019), requiring the blueschist facies metabasites to be decoupled from the subducting oceanic slab but reside in the subduction zone for ~ 25 Myr.

The timing of the blueschist facies events in the middle (c. 364 Ma) and lower (c. 345–336.5 Ma) allochthons bracket the occurrence of epidote–amphibolite facies metamorphism in the LMC (350.1 ± 5.3 Ma; Fig. 8). The LMC has previously been interpreted as a relic of the Saxothuringian Ocean (Narębski et al. 1986; Szałamacha and Szałamacha 1991; Mazur and Aleksandrowski 2001). This interpretation would require it to trail, or be directly associated with, the lower allochthon rocks into the subduction zone, as epidote–amphibolite metamorphism was slightly (~ 8 Myr) older than blueschist facies metamorphism of the lower allochthon. However, this geometry brings forth several complications: (1) The LMC would have to represent ocean crust directly below or behind the lower allochthon passive margin rocks, yet were decoupled from the subducting slab in medium pressure conditions without decoupling of the lower allochthon rocks; (2) It would require the lower and middle allochthons to be separated from the Saxothuringian terrane by a hyper-extended margin, yet the metaigneous complex lacks any rift-related sedimentary rocks; (3) This progression would not explain the different orientations of L1 for the LMC versus the lower and middle allochthons without a major shift in subduction vergence; (4) The geometry of the LMC below or behind the lower allochthon creates a complex geometry for exhumation of the Karkonosze-Izera Massif, as the LMC would have to overthrust the lower and middle allochthons, or be repositioned after exhumation by out-of-sequence thrusting without reorienting the vergence of L2 in the LMC.

It is likely that the LMC originated as part of the overriding Teplá-Barrandian Domain (Konopásek et al. 2019), rather than a relic of the Saxothuringian Ocean or hyper-extended passive margin (Mazur and Aleksandrowski 2001). In such a scenario (Fig. 9), the LMC would have been entrained into the subduction zone via subduction erosion of lower crust (e.g., Stern 2020; Satish-Kumar et al. 2021).

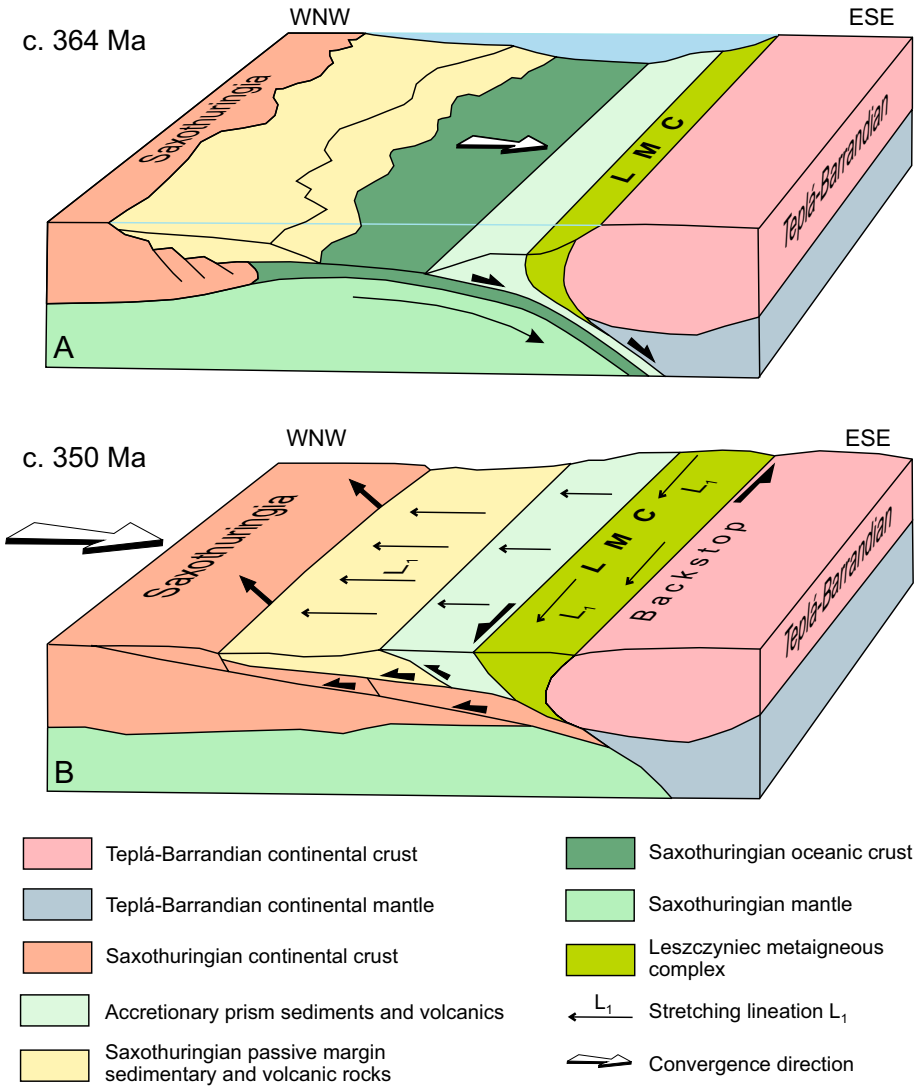


**Fig. 9** Interpretation diagram illustrating the geodynamic scenario based on the present results and previous studies. **a** The Leszczyniec metaigneous complex entrained into the subduction zone via subduction erosion of the upper plate. Accretionary prism and subduction channel rocks include metabasites decoupled from the subducting oceanic slab (future component of the middle allochthon) that experienced blueschist facies metamorphism. Sedimentary rocks of the Saxothuringian passive margin contain protoliths of the future lower allochthon and part of the middle allochthon. **b** Transition from oceanic to continental subduction, following the demise of the Saxothuringian Ocean. Intense E–W shortening in front of the Teplá-Barrandian backstop, leads to the steep N-S trending fabric in the Leszczyniec metaigneous complex with stretching direction perpendicular to the E-W tectonic transport. *LMC* Leszczyniec metaigneous complex

The different orientation of L1 with respect to the subjacent allochthons would indicate left-lateral movement of the complex in the subduction zone during subduction erosion, possibly reflecting heterogeneity of the Saxothuringian Ocean/margin along strike of the subduction zone producing lateral compressional gradients. Alternatively, the 350 Ma ages may be associated with intense E-W shortening, leading to the steep N-S trending fabric with stretching perpendicular to the E-W transport (Fig. 9). Regardless of the kinematic scenario responsible for the development of the N-S fabric, the LMC would also be positioned structurally above the lower and middle allochthon rocks (Fig. 9), allowing for the current tectonostratigraphy to be achieved with a concordant L2 orientation and vergence for all allochthons. Consequently, the tectonic suture separating the Saxothuringian and Teplá-Barrandian domains is located within the composite middle allochthon of the Karkonosze-Izera Massif. The suture separates rocks derived from an accretionary prism or subduction channel recorded as blueschist facies metabasites (Patočka and Pin 2005) from those coming from the distal Saxothuringian passive margin (Winchester et al 2003). At a larger scale, this tectonic contact corresponds to a boundary between the upper and middle Variscan allochthons differentiated by Martínez Catalán et al. (2020). The ages obtained demonstrate that the Teplá-Barrandian upper plate avoided a thermal overprint related to exhumation of the Variscan accretionary wedge between 335 and 320 Ma.

## Conclusions

In situ white mica Rb/Sr geochronology was performed on two felsic orthogneisses from an outcrop of the LMC in the Karkonosze-Izera Massif, West Sudetes. The orthogneisses exhibit a well-developed foliation and stretching lineation that are defined by alignment of white mica and

recrystallized quartz. These structures are related to epidote–amphibolite facies metamorphism of the complex. Single-spot white mica Rb/Sr dates were calculated for the two orthogneisses using initial $^{87}Sr/^{86}Sr$ values obtained from titanite and epidote concomitant with white mica. The two orthogneisses yielded different initial $^{87}Sr/^{86}Sr$ (LC22-05: $0.7034 \pm 0.0028$; LC22-06: $0.7083 \pm 0.0037$) but comparable single-spot dates with overlapping weighted averages of $352.4 \pm 4.1$ Ma (LC22-05) and $349.3 \pm 2.5$ Ma (LC22-06). These weighted averages are similar, but with higher precision, to isochron dates from the same results that were calculated without initial $^{87}Sr/^{86}Sr$ values. White mica in both orthogneisses are interpreted to record (re)crystallization during epidote–amphibolite facies metamorphism and development of the associated foliation and stretching lineation. Therefore, a pooled weighted average from the results of both rocks of $350.1 \pm 5.3$ Ma ($2\sigma$) is reported for the timing of the event.

The timing of epidote–amphibolite facies metamorphism of the LMC is bracketed by the timing of blueschist facies metamorphism of metabasites in the subjacent middle allochthon (c. 364 Ma) and lower allochthon (c. 345–336.5 Ma) rocks that represent relics of the subducted oceanic crust and the Saxothuringian passive margin, respectively. Considering the structural fabrics, ages and conditions of metamorphism, and the inferred geometry of the Saxothuringian passive margin, it is proposed that the LMC did not originate from the Saxothuringian Ocean or passive margin, but rather was derived from the overriding Teplá-Barrandian Domain via subduction erosion. The origin of the LMC implies that the suture separating the Saxothuringian and Teplá-Barrandian domains is contained within the middle allochthon of the Karkonosze-Izera Massif, separating blueschist facies metabasites, derived from an accretionary prism or subduction channel, from rocks representing the distal margin of the Saxothuringian terrane. The growth of the N–S oriented fabric in the LMC, including lineation L1, at 350 Ma could have reflected the transition from oceanic to continental subduction, following the demise of the Saxothuringian Ocean.

**Supplementary Information** The online version contains supplementary material available at https://doi.org/10.1007/s00531-023-02373-8.

**Acknowledgements** The following people are thanked for their assistance: D. Rösel with in situ Rb/Sr geochronology and M. Ponikowska with fieldwork and sample collection, U. Riller and K. Schulmann for their editorial handling and comments, and P. Jeřábek and an anonymous reviewer for their reviews that were helpful for improving the quality and presentation of the work. This work was supported by the Polish National Science Centre Grant No. 2016/23/N/ST10/01296 awarded to Maria Młynarska.

**Data availability** All data is available supplementary files. The spreadsheet used to recalculate LA-ICP-MS/MS white mica chemistry is available upon request to the corresponding author.

## Declarations

**Conflict of interest** There are no financial nor non-financial competing interests to disclose.



## References

Chaloupský J (ed) (1989) Geology of the Krkonoše and Jizerské hory Mts. Ustřední Ústav Geologický, Praha **(in Czech, English summary)**

Chlupáč I (1993) Stratigraphic evaluation of some metamorphic units in the N part of the Bohemian Massif. Neues Jb Geol Paläontol Abh 188:363–388

Clemens JD, Stevens G, Coetzer LM (2023) Dating initial crystallization of some Devonian plutons in central Victoria and geological implications. Aust J Earth Sci 70:60–72. https://doi.org/10.1080/08120099.2022.2106513

Coggon R, Holland TJB (2002) Mixing properties of phengitic micas and revised garnet-phengite thermobarometers. J Metamorph Geol 20:683–696. https://doi.org/10.1046/j.1525-1314.2002.00395.x

Faryad SW, Kachlík V (2013) New evidence of blueschist facies rocks and their geotectonic implication for Variscan suture(s) in the Bohemian Massif. J Metamorph Geol 31:63–82. https://doi.org/10.1111/jmg.12009

Franke W, Żelaźniewicz A, Porębski SJ, Wajsprych B (1993) Saxothuringian zone in Germany and Poland: differences and common features. Geol Rundsch 82(3):583–599. https://doi.org/10.1007/BF00212418

Franke W, Żelaźniewicz A (2000) The eastern termination of the Variscides: terrane correlation and kinematic evolution. In: Franke W, Haak V, Oncken O, Tanner D (eds), Quantification and Modelling in the Variscan Belt, vol 179. Geological Society, London, Special Publication, pp 63–86. https://doi.org/10.1144/GSL.SP.2000.179.01.06

Glodny J, Grauert B, Fiala J, Vejnar Z, Krohe A (1998) Metapegmatites in the western Bohemian massif: ages of crystallization and metamorphic overprint, as constrained by U-Pb zircon, monazite, garnet, columbite and Rb-Sr muscovite data. Geol Rundsch 87:124–134. https://doi.org/10.1007/s005310050194

Grove M, Harrison TM (1996) $^{40}Ar^*$ diffusion in Fe-rich biotite. Am Miner 81:940–951

Hogmalm KJ, Zack T, Karlsson AK-O, Sjoqvist ASL, Garbe-Schonberg D (2017) *In situ* Rb-Sr and K-Ca dating by LA-ICP-MS/MS: an evaluation of $N_2O$ and $SF_6$ as reaction gases. J Anal at Spectrom 32:305–313. https://doi.org/10.1039/C6JA00362A

Hu Z, Liu Y, Gao S, Xiao S, Zhao L, Gunther D, Li M, Zhang W, Zong K (2012) A "wire" signal smoothing device for laser ablation inductively coupled plasma-mass spectrometry analysis. Spectrochim Acta Part B at Spectrom 78:50–57. https://doi.org/10.1016/j.sab.2012.09.007

Jeřábek P, Konopásek J, Žáčková E (2016) Two-stage exhumation of subducted Saxothuringian continental crust records underplating in the subduction channel and collisional forced folding (Krkonoše-Jizera Mts., Bohemian Massif). J Struct Geol 89:214–229. https://doi.org/10.1016/j.jsg.2016.06.008

Kachlík V, Kozdrój W (2001) Ještěd Range Unit. In: Kozdrój W, Krentz O, Opletal M (eds) Comments on the Geological map Lauzitz–Jizera–Karkonosze (without Cenozoic sediments). Sächsisches Landesamt für Umwelt und Geologie/Bereich Boden und Geologie, Freiberg, Państwowy Instytut Geologiczny, Warszawa. Český geolologický ústav Praha, pp 27–31

Konopásek J, Anczkiewicz R, Jeřábek P, Corfu F, Žáčková E (2019) Chronology of the Saxothuringian subduction in the West Sudetes (Bohemian Massif, Czech Republic and Poland). J Geol Soc 176(3):492–504. https://doi.org/10.1144/jgs2018-173

Kozdrój W, Turniak K, Tichomirova M, Bombach K, Kachlík V, Ziółkowska-Kozdrój M (2005) New 207Pb/206Pb zircon ages from the East Karkonosze Metamorphic Complex, West Sudetes–evidence of the Late Cambrian-Early Ordovician magmatism. Geolines 19:69–70

Kröner A, Jaeckel P, Hegner E, Opletal M (2001) Single zircon ages and whole-rock Nd isotopic systematics of early Palaeozoic granitoid gneisses from the Czech and Polish Sudetes (Jizerské hory, Krkonoše and Orlice-Sněžnik Complex). Int J Earth Sci 90:304–324. https://doi.org/10.1007/s005310000139

Kryza R, Mazur S (1995) Contrasting metamorphic paths in the SE part of the Karkonosze-Izera block (Western Sudetes, SW Poland). Neues Jb Mineral Abh 169:157–192

Kryza R, Mazur S, Pin C (1995) Leszczyniec meta-igneous complex in the eastern part of the Karkonosze-Izera Block, Western Sudetes: trace element and Nd isotope study. Neues Jb Geol Paläontol Abh 170:59–74

Kryza R, Schaltegger U, Oberc-Dziedzic T, Pin C, Ovtcharova M (2014) Geochronology of a composite granitoid pluton: a high-precision ID-TIMS U-Pb zircon study of the Variscan Karkonosze Granite (SW Poland). Int J Earth Sci 103(3):683–696. https://doi.org/10.1007/s00531-013-0995-0

Li Q-L, Chen F, Li X-H, Wang F, He H-Y (2008) Single grain Rb–Sr isotopic analysis of GA-1550 biotite, LP-6 biotite and Bern-4M muscovite $^{40}$Ar–$^{39}$Ar dating standards. Geochem J 42:263–271. https://doi.org/10.2343/geochemj.42.263

Machowiak K, Armstrong R (2007) SHRIMP U-Pb zircon age from the Karkonosze granite. Mineral Pol Spec Pap 31:193–196

Majka J, Mazur S, Kośmińska K, Dudek K, Klonowska I (2016) Pressure–temperature estimates of the blueschists from the Kopina Mt., northern Bohemian Massif, Poland–constraints on subduction of the Saxothuringian continental margin. Eur J Mineral 28(6):1047–1057. https://doi.org/10.1127/ejm/2016/0028-2601

Malusky H, Patočka F (1997) Geochemistry and 40Ar-39Ar geochronology of the mafic metavolcanic rocks from the Rýchory Mountains complex (west Sudetes, Bohemian Massif): paleotectonic significance. Geol Mag 134(5):703–716. https://doi.org/10.1017/S0016756897007498

Marheine D, Kachlík V, Maluski H, Patočka F, Zelazniewicz A (2002) The 40Ar/39Ar ages from the West Sudetes (NE Bohemian Massif): constraints on the Variscan polyphase-tectonothemal development. In: Winchester J, Pharaoh T, Verniers J (eds) Palaeozoic amalgamation of Central Europe. Geological Society, London, Special Publication, vol 201, pp 133–155. https://doi.org/10.1144/GSL.SP.2002.201.01.07

Martínez Catalán JR, Collett S, Schulmann K, Aleksandrowski P, Mazur S (2020) Correlation of allochthonous terranes and major tectonostratigraphic domains between NW Iberia and the Bohemian Massif, European Variscan belt. Int J Earth Sci 109:1105–1131. https://doi.org/10.1007/s00531-019-01800-z

Massonne H-J, Schreyer W (1987) Phengite geobarometry based on the limiting assemblage with K-feldspar, phlogopite, and quartz. Contrib Miner Petrol 96:212–224

Mazur S, Aleksandrowski P (2001) The Teplá(?)/Saxothuringian suture in the Karkonosze-Izera massif, Western Sudetes, Central European Variscides. Int J Earth Sci 90:341–360. https://doi.org/10.1007/s005310000146

Mazur S, Kryza R (1996) Superimposed compressional and extensional tectonics in the Karkonosze-Izera Block, NE Bohemian Massif. In: Oncken O, Janssen C (eds) Basement tectonics 11, Europe and Other Regions. Potsdam, Kluwer, Dordrecht, pp 51–66. https://doi.org/10.1007/978-94-009-1598-5_4

Mazur S (1995) Structural and metamorphic evolution of the country rocks at the eastern contact of the Karkonosze granite in the southern Rudawy Janowickie Mts and Lasocki Range. Geol Sudet 29:31–98 **(in Polish, English summary)**

Narębski W (1994) Lower to Upper Paleozoic tectonomagmatic evolution of NE part of the Bohemian Massif. Zentralblatt Geol Paläontol I:961–972

Narębski W, Dostal J, Dupuy C (1986) Geochemical characteristics of Lower Paleozoic spilite–keratophyre series in the Western Sudetes (Poland): petrogenetic and tectonic implications. Neues Jb Mineral Abh 155:243–258

Oberc-Dziedzic T, Kryza R, Mochnacka K, Larionov A (2010) Ordovician passive continental margin magmatism in the Central-European Variscides: U-Pb zircon data from the SE part of the Karkonosze-Izera Massif, Sudetes, SW Poland. Int J Earth Sci 99:27–46. https://doi.org/10.1007/s00531-008-0382-4

Oliver GJH, Corfu F, Krough TE (1993) U-Pb ages from SW Poland: evidence for a Caledonian suture zone between Baltica and Gondwana. J Geol Soc Lond 150:355–369. https://doi.org/10.1144/gsjgs.150.2.0355

Patočka F, Pin C (2005) Sm-Nd isotope and trace element evidence for heterogeneous igneous protoliths of Variscan mafic blueschists in the East Krkonoše Complex (West Sudetes, NE Bohemian Massif, Czech Republic). Geodin Acta 18(5):363–374. https://doi.org/10.3166/ga.18.363-374

Paton C, Hellstrom J, Paul B, Woodhead J, Hergt J (2011) Iolite: Freeware for the visualization and processing of mass spectrometric data. J Anal Spectrom 26:2508–2518

Phillips D, Matchan EL, Honda M, Kuiper KF (2017) Astronomical calibration of $^{40}$Ar/$^{39}$Ar reference minerals using high-precision, multi-collector (ARGUSVI) mass spectrometry. Geochim Cosmochim Acta 196:351–369

Redaa A, Farkaš J, Gilbert S, Collins AS, Löhr S, Vasegh D, Forster M, Blades M, Zack T, Giuliani A, Maas R, Baldermann A, Dietzel M, Garbe-Schönberg D (2022) Testing nano-powder and fused-glass mineral reference materials for *in situ* Rb-Sr dating of glauconite, phlogopite, biotite and feldspar via LA-ICP-MS/MS. Geostand Geoanal Res. https://doi.org/10.1111/ggr.12467

Romer RL, Smeds S-A (1994) Implications of U-Pb ages of columbite-tantalites from granitic pegmatites for the Palaeoproterozoic accretion of 1.90–1.85 Ga magmatic arcs to the Baltic Shield. Precambr Res 67:141–158

Rösel D, Zack T (2022) LA-ICP-MS/MS single-spot Rb-Sr dating. Geostand Geoanal Res 46:143–168. https://doi.org/10.1111/ggr.12414

Rosenberg CL, Stünitz H (2003) Deformation and recrystallization of plagioclase along a temperature gradient: an example from the Bergell tonalite. J Struct Geol 25(3):389–408. https://doi.org/10.1016/S0191-8141(02)00036-6

Satish-Kumar M, Kurihara T, Shishido R, Yoshida T, Takahashi T, Nohara-Imanaka R (2021) Geochemistry and Sr–Nd isotopic composition of meta-gabbros from the Omi serpentinite mélange, Niigata, SW Japan: Evidence for subduction erosion

in an immature early Paleozoic arc-trench system in proto-Japan. Lithos 398:106260. https://doi.org/10.1016/j.lithos.2021.106260
Schoene B, Crowley JL, Condon DJ, Schmitz MD, Bowring SA (2006) Reassessing the uranium decay constants for geochronology using ID-TIMS U-Pb data. Geochim Cosmochim Acta 70:426–445
Smulikowski W (1995) Evidence for glaucophane-schist facies metamorphism in the East Karkonosze complex, West Sudetes, Poland. Geol Rundsch 84:720–737. https://doi.org/10.1007/BF00240563
Stern CR (2020) The role of subduction erosion in the generation of Andean and other convergent plate boundary arc magmas, the continental crust and mantle. Gondwana Res 88:220–249. https://doi.org/10.1016/j.gr.2020.08.006
Stipp M, Stünitz H, Heilbronner R, Schmid SM (2002) Dynamic recrystallization of quartz: correlation between natural and experimental conditions. In: De Meer S, Drury MR, De Bresser JHP, Pennock GM (eds) Deformation mechanisms, rheology and tectonics: current status and future perspective, vol 200. Geological Society, London, Special Publications, pp 171–190. https://doi.org/10.1144/GSL.SP.2001.200.01.11
Szałamacha M, Szałamacha J (1991) Ofiolit Leszczyńca w Rudawach Janowickich. Biuletyn Instytutu Geologicznego 367:61–84
Vermeesch P (2018) IsoplotR: a free and open toolbox for geochronology. Geosci Front 9:1479–1493. https://doi.org/10.1016/j.gsf.2018.04.001
Waight TE, Maas R, Nicholls IA (2000) Fingerprinting feldspar phenocrysts using crystal isotopic composition stratigraphy: implications for crystal transfer and magma mingling in S-type granites. Contrib Miner Petrol 139:227–239
Williams IS, Tetley NW, Compston W, McDougall I (1982) A comparison of K-Ar and Rb-Sr ages of rapidly cooled igneous rocks: Two points in the Palaeozoic time scale reevaluated. J Geol Soc Lond 139:557–568
Winchester JA, Floyd PA, Chocyk M, Horbowy K, Kozdrój W (1995) Geochemistry and tectonic environment of Ordovician meta-igneous rocks in the Rudawy Janowickie Complex, SW Poland. J Geol Soc Lond 152:105–115. https://doi.org/10.1144/gsjgs.152.1.0105
Winchester JA, Patočka F, Kachlik V, Melzer M, Nawakowski C, Crowley QG, Floyd PA (2003) Geochemical discrimination of metasedimentary sequences in the Krkonoše-Jizera Terrane (West Sudetes, Bohemian Massif): paleotectonic and stratigraphic constraints. Geol Carpath 54(5):267–280
Zack T, Hogmalm KJ (2016) Laser ablation Rb/Sr dating by online chemical separation of Rb and Sr in an oxygen-filled reaction cell. Chem Geol 437:120–213. https://doi.org/10.1016/j.chemgeo.2016.05.027
Žáčková E, Konopásek J, Jeřábek P, Finger F, Košler J (2010) Early Carboniferous blueschist facies metamorphism in metapelites of the West Sudetes (northern Saxothuringian Domain, Bohemian Massif). J Metamorph Geol 28(4):361–379. https://doi.org/10.1111/j.1525-1314.2010.00869.x
Žák J, Verner K, Sláma J, Kachlík V, Chlupáčová M (2013) Multistage magma emplacement and progressive strain accumulation in the shallow-level Krkonoše-Jizera plutonic complex. Bohemian Massif Tecton 32(5):1493–1512. https://doi.org/10.1002/tect.20088
Zieger J, Linnemann U, Hofmann M, Gärtner A, Marko L, Gerdes A (2018) A new U-Pb LA-ICP-MS age of the Rumburk granite (Lausitz Block, Saxo-Thuringian Zone): constraints for a magmatic event in the Upper Cambrian. Int J Earth Sci 107(3):933–953. https://doi.org/10.1007/s00531-017-1511-8